

Origin of termination of negative-parity bands

G. G. Adamian,¹ N. V. Antonenko,^{1,2} and H. Lenske³

¹*Joint Institute for Nuclear Research, 141980 Dubna, Russia*

²*Mathematical Physics Department, Tomsk Polytechnic University, Lenin Avenue 30, 634050 Tomsk, Russia*

³*Institut für Theoretische Physik der Justus-Liebig-Universität, D-35392 Giessen, Germany*

(Received 12 September 2015; published 23 November 2015)

The cluster approach is applied to study the mechanism of termination of the negative-parity band built on the ground state of even-even nucleus. For the several even-even nuclei, the terminating spins are predicted. The method is suggested for the verification of the cluster interpretation of the band termination.

DOI: [10.1103/PhysRevC.92.054319](https://doi.org/10.1103/PhysRevC.92.054319)

PACS number(s): 21.60.Ev, 21.60.Gx

I. INTRODUCTION

The low-lying negative-parity states observed in pre-actinides, actinides, medium-mass isotopes, and light nuclei are definitely related to reflection-asymmetric shapes [1]. There are several approaches [2–12] based on the assumption that the reflection-asymmetric shape is the consequence of clustering in nuclei. In the algebraic model [4,11] an alpha clusterization was employed to describe the properties of alternative-parity bands. In Refs. [7–9] a di-cluster configuration with a lighter cluster ${}^4\text{He}$ or heavier than ${}^4\text{He}$ was used. In both models [4,11] and [7–9] the relative distance R between the centers of mass of clusters at fixed mass asymmetry is the main collective coordinate for the description of the low-lying positive and negative parity states. In the model [7–9] the cluster is viewed as a single particle in a certain orbit with principal quantum number n of relative motion (the number of interior nodes in the radial wave function) and orbital quantum number L . The cluster and core penetrate each other because the relative distance between them can be smaller than the sum of cluster and core radii, $R_1 + R_2$. The spectroscopic factor of clustering is equal to unity even at small spins. The cluster-core Schrödinger equation in R with a deep local double-folding potential and the Pauli principle allowed for by a projection was successfully employed in [7–9] to describe the properties of the states of the alternating parity bands (energy spectra, transition probabilities) and widths of the alpha- [13] and light-cluster decays. The main requirements of the Pauli exclusion principle are satisfied by choosing the quantum numbers n and L to obey a Wildermuth condition, $2n + L \geq N$, where N is a constant integer chosen large enough to correspond to a microscopic situation in which the cluster nucleons all occupy orbitals above those already occupied by the core nucleons [7]. Because each cluster band belongs to a particular value of the single-particle harmonic oscillator excitation quanta N , one can easily determine the band termination spin.

In the framework of the cluster model [14–19] the dependencies of parity splitting and multipole $E1$, $E2$, and $E3$ transition moments on spin in the alternating parity bands built on the ground states of even and odd medium-mass and heavy nuclei have been successfully described. The model was applied to describe the alpha decays, cluster radioactivity, population, and decay-out of the superdeformed bands [17–20]. This cluster model is based on the assumption that the reflection-

asymmetric shapes are produced by the collective motion of the nuclear system in the mass (charge) asymmetry coordinate $\eta = (A_1 - A_2)/(A_1 + A_2)$ ($\eta_Z = (Z_1 - Z_2)/(Z_1 + Z_2)$), where A_1 (Z_1) and A_2 (Z_2) are the mass (charge) numbers, respectively, of the clusters. Here the molecularlike cluster systems are two touching clusters with a relative distance about $R_m = R_1 + R_2 + 0.5$ fm (the touching configuration), which corresponds to the minimum of the shallow effective cluster-cluster interaction potential. The antisymmetrization between nucleons belonging to different clusters is allowed for by a density dependence of the nucleon-nucleon force which gives a repulsive core in the cluster-cluster interaction potential. The relative weights of each cluster and clusterless (mononucleus) components in the wave function $\Psi_J(\eta)$ are determined by solving the stationary Schrödinger equation,

$$(T + U)\Psi_J(\eta) = E_J\Psi_J(\eta),$$

in the mass (charge) asymmetry coordinate with the kinetic T and potential,

$$U(\eta, R_m, J, \beta_i) = B_1 + B_2 + V(R_m, J, \beta_i),$$

energies. Here, U is equal to the sum of the binding energies B_i ($i = 1, 2$) of clusters and the cluster-cluster interaction V which contains the rotational energy. Because the potential energy is invariant under the inversion $\eta \rightarrow -\eta$, every non-degenerate eigenfunction $\Psi_J(\eta)$ has a definite parity. The rotational states are built on the vibrational states in η . In the case of the even-even nuclei we have a set of states with $J^\pi = 0^+, 1^-, 2^+, 3^-, 4^+, \dots$; i.e., the positive and negative rotational bands are built on the lowest even and odd states in η , respectively. So, the positive and negative-parity states are treated on the same footing [14–19]. Note that the low-lying positive-parity rotational states are mainly described by the mononucleus component (clusterless configuration).

Because the energies of cluster configurations with a light cluster heavier than the α -particle increase rapidly with decreasing η (η_Z), the energetically favorable ${}^4\text{He}$ -cluster configuration ${}^AZ \rightarrow {}^{A-4}(Z-2) + {}^4\text{He}$ gives the main contribution in the wave function $\Psi_J(\eta)$ [14–19]. In the low-lying negative-parity rotational states with high spins, the value of the α -particle spectroscopic factor becomes close to unity. At small spins, the spectroscopic factor is less than unity. Thus, it could be argued that the reflection-asymmetric

shape, especially at the high spins, is a consequence of alpha clustering in the nucleus.

If the cluster model [14–19] gives a good quantitative explanation of the observed properties of the lowest-lying negative-parity bands, this collective model can serve as a good ground for the description and better understanding of the mechanism of termination of these bands. The cluster configuration is located in the minimum of the potential pocket of the cluster-cluster interaction potential. Because the centrifugal potential acts repulsively and enforces this minimum, for values J larger than the critical angular momentum J_{\max} , the pocket vanishes (its depth becomes zero) and the di-cluster system becomes unbound and easily decays into two fragments. However, even at $J \leq J_{\max}$ the cold (the internal excitation energy is zero) rotating dinuclear system (DNS) may decay into two fragments (α decay) by tunneling through the potential barrier. So, at high spins the $E2$ transition between negative-parity states competes with α decay. With increasing J the α -decay time $T_\alpha(J)$ becomes comparable and then smaller than the γ -transition time $T_\gamma(J)$. One can expect that the terminating spins J_{term} [$J_{\text{term}} < J_{\max}$] for the ${}^A Z \rightarrow {}^{A-4}(Z-2) + {}^4\text{He}$ cluster configuration is determined from the condition,

$$T_\alpha(J_{\text{term}}) \ll T_\gamma(J_{\text{term}}). \quad (1)$$

Thus, at $J \geq J_{\text{term}}$ the cold cluster configuration ${}^A Z \rightarrow {}^{A-4}(Z-2) + {}^4\text{He}$ is unstable and, correspondingly, the related low-lying negative-parity band does not exist. The negative-parity band disappears upon reaching this terminating state with $J = J_{\text{term}}$. One can say that the physical origin of the termination of the negative-parity rotational band built on the ground state is the alpha decay, the observation of which allows us to verify whether the cluster interpretation is suitable for the low-lying negative-parity states. The other consequence of the α clustering and α decay is that because the alpha-cluster spectroscopic factor in the state with even spin is smaller than in the neighboring states with odd spins, the termination spin of the positive-parity band built on the ground state must be larger than the one of the lowest negative-parity band.

II. MODEL

To calculate the termination spin J_{term} , we use the cluster-cluster (nucleus-nucleus) interaction potential [14–19,21],

$$V(R, J, \beta_i) = V_C + V_N + \hbar^2 J(J+1)/(2\mathfrak{I}). \quad (2)$$

It is given as the sum of the Coulomb potential V_C , the nuclear potential V_N , and the centrifugal potential (last summand) with the moment of inertia \mathfrak{I} of the DNS formed. In our notations R , μ , and β_i ($i = 1, 2$) are the relative distance between the centers of mass of clusters, reduced mass parameter, and the quadrupole deformation parameters of the clusters, respectively. For the nuclear part, we use the double-folding formalism with the Skyrme-type effective density-dependent nucleon-nucleon interaction [21]. The parameters of the nucleon-nucleon interaction are fixed in nuclear structure calculations [22]. The densities of the nuclei are taken in the Woods-Saxon form with the nuclear radius parameters $r_0 = 1.02$ and 1.15 fm and the diffuseness parameters $a = 0.48$

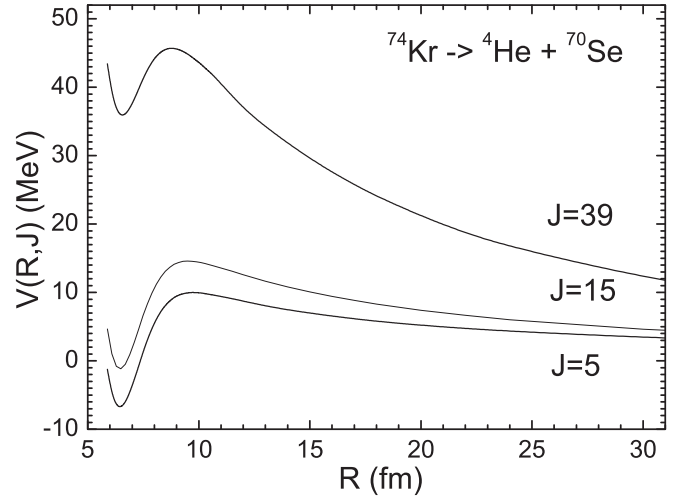


FIG. 1. Nucleus-nucleus interaction potential for the ${}^4\text{He} + {}^{70}\text{Se}$ system at indicated angular momenta.

and 0.53 – 0.55 fm for the alpha particle and heavy cluster (depending on the mass and charge numbers), respectively. The relative orientation of the deformed clusters in the dinuclear system follows the minimum of the potential energy which results in the sphere-to-pole or pole-to-pole orientation. The absolute values of the quadrupole deformation parameters β_i of the deformed nuclei are taken from Ref. [23]. For the double magic and semimagic nuclei, we take $\beta_i = 0$.

The value of \mathfrak{I} is calculated in the sticking limit as

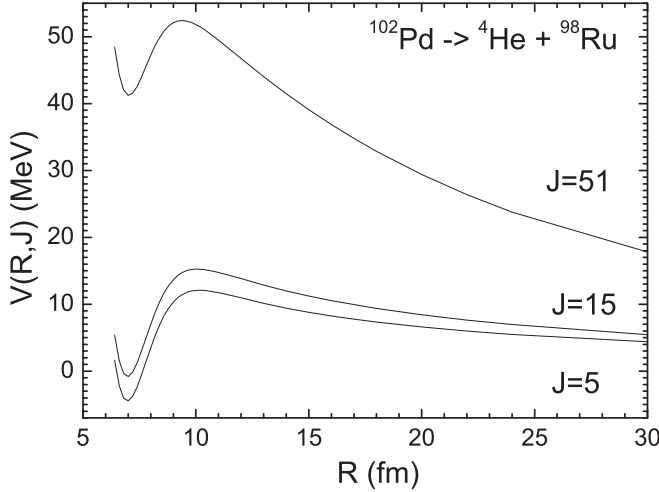
$$\mathfrak{I}(R, \beta_i) = k_0(\mathfrak{I}_1 + \mathfrak{I}_2 + \mu R^2). \quad (3)$$

For large angular momenta J , the moments of inertia \mathfrak{I}_i ($i = 1, 2$) of the DNS nuclei are obtained in the rigid body approximation. As known from the experimental study, the moments of inertia of strongly deformed nuclear states are close to 85% of those in the rigid body limit [24]. We also set $k_0 = 0.85$ in our calculations. With Eq. (3) the values of \mathfrak{I} at $R = R_m$ are in a good agreement with those extracted from the experimental spectra. The smaller the value of \mathfrak{I}_m , the smaller value of J_{term} .

The nucleus-nucleus interaction potentials V versus R are presented in Figs. 1 and 2 at different values of angular momentum J . As a result of the density-dependent nucleon-nucleon interaction used in the calculation of V , a repulsive core appears which prevents the motion to smaller R and represents the Pauli principle. Because of the sum of the repulsive Coulomb and centrifugal summands with the attractive nuclear one in Eq. (2), the nucleus-nucleus potential has a potential pocket with a minimum situated at the distance $R = R_m \approx R_1(\beta_1) + R_2(\beta_2) + 0.5$ fm, where R_i are the radii of clusters. The cluster system is localized in the minimum of this pocket at $R = R_m$. The position of the Coulomb barrier corresponds to $R = R_b \approx R_m + (3.2\text{--}3.8)$ fm at $J = 0$ in the cluster configurations considered. Then the depth of the potential pocket is

$$B_R^{qf}(J) = V(R_b, J, \beta_i) - V(R_m, J, \beta_i). \quad (4)$$

The barrier B_R^{qf} prevents the cluster system decay in R . So, the stability of the cluster system is governed by the value of B_R^{qf} .


 FIG. 2. The same as in Fig. 1, but for the ${}^4\text{He} + {}^{98}\text{Ru}$ system.

The depth B_R^{qf} of the potential pocket decreases with increasing J because of the growth of the repulsive centrifugal part of the nucleus-nucleus potential (2) and vanishes at $J > J_{\max}$. For the systems ${}^4\text{He} + {}^{70}\text{Se}$ and ${}^4\text{He} + {}^{98}\text{Ru}$, $J_{\max}=45$ and 111, respectively. One can see in Figs. 1 and 2 that for the ${}^4\text{He} + {}^{70}\text{Se}$ (${}^4\text{He} + {}^{98}\text{Ru}$) the value of B_R^{qf} decreases by 6.9 MeV (5.45 MeV) with increasing J from 5 to 39 (51).

Using the values of Im and the electric quadrupole moment of the DNS [$Q_2^{(c)}(i)$ ($i = 1, 2$) are the quadrupole moments of the DNS nuclei] [25],

$$Q_2^{(c)} = 2e \frac{A_2^2 Z_1 + A_1^2 Z_2}{A^2} R_m^2 + Q_2^{(c)}(1) + Q_2^{(c)}(2),$$

we obtain the energy $E_\gamma(J \rightarrow J-2) = J(J+1)/(2\mathfrak{I}) - (J-2)(J-1)/(2\mathfrak{I}) = (2J-1)/\mathfrak{I}$ and the time $T_\gamma(J)$ of the collective $E2$ transition between the rotational states with J and $J-2$ as in Ref. [23]:

$$T_\gamma(J) = \frac{408.1}{\frac{5}{16\pi} [Q_2^{(c)}]^2 [E_\gamma(J \rightarrow J-2)]^5}, \quad (5)$$

where E_γ is in units of keV, $Q_2^{(c)}$ in $10^2(e \text{ fm}^2)$, and T_γ in s.

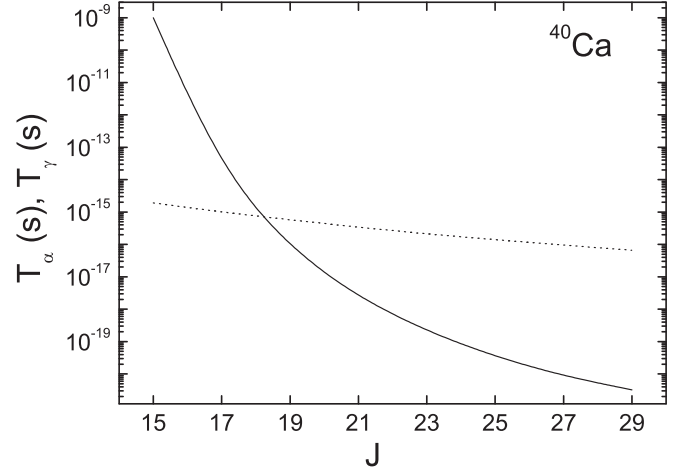
The process which competes with γ emission is tunneling through the barrier in R (α decay). By employing the WKB approach, the tunneling time through the barrier in R is estimated as

$$T_\alpha(J) = \frac{2\pi}{\omega_m(J)} (1 + \exp[2S_\alpha(J)/\hbar]), \quad (6)$$

where

$$S_\alpha(J) = \int_{R_m}^{R_{ex}} dR (2\mu[V(R, J, \beta_i) - E_{c.m.}])^{1/2}$$

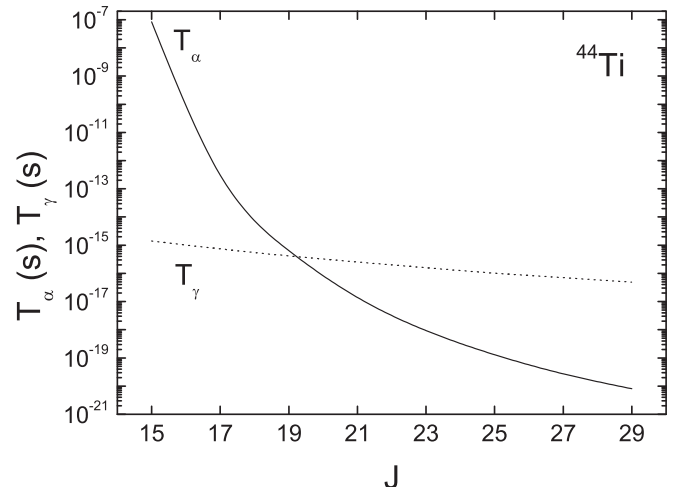
is the classical action in R , R_{ex} is the external turning point, and $\omega_m = \sqrt{\partial^2 V / \partial R^2}|_{R=R_m} / \mu$ is the assault frequency in the potential pocket at a given value of J .


 FIG. 3. Times of $E2$ transition and α decay as functions of angular momentum J for the indicated nucleus.

III. CALCULATION RESULTS

The condition (1) sufficiently restricts the interval of angular momenta at which one can identify states of the negative-parity band.

As seen from (5), the value of T_γ mainly depends on J through E_γ . The angular momentum dependence of T_α are determined by the angular momentum dependence of the Coulomb barrier. The value of the barrier height B_R^{qf} decreases with increasing contribution of the repulsive centrifugal part in Eq. (2) (see Figs. 1 and 2). As examples, the values of T_γ and T_α as functions of J are presented in Figs. 3–6 for the systems ${}^4\text{He} + {}^{36}\text{Ar}$, ${}^4\text{He} + {}^{40}\text{Ca}$, ${}^4\text{He} + {}^{58}\text{Ni}$, and ${}^4\text{He} + {}^{70}\text{Se}$. The two curves cross each other and the condition $T_\alpha \ll T_\gamma$ is valid only at high J when the value of B_R^{qf} considerably decreases. Near this crossing point the γ - and α -decay probabilities become comparable. Thus, one can see from the analysis of Figs. 3–6 that the α -cluster nature of the negative-parity states can be identified by measuring the rotational γ quanta in coincidence


 FIG. 4. Times of $E2$ transition and α decay as functions of angular momentum J for the indicated nucleus.

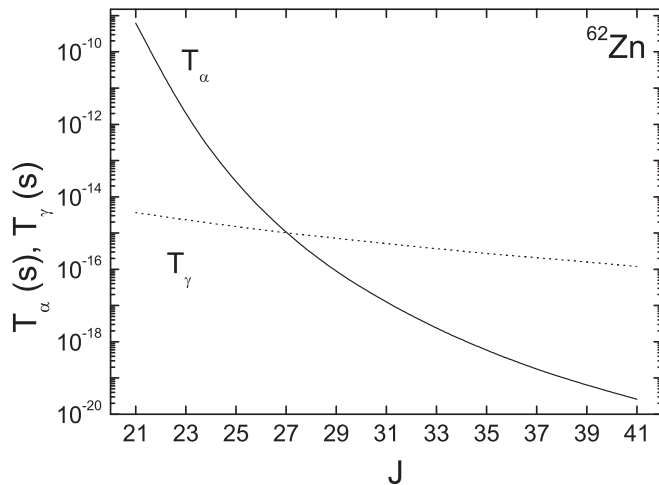


FIG. 5. Times of $E2$ transition and α decay as functions of angular momentum J for the indicated nucleus.

with the α -decay fragments at J corresponding to the vicinity of the crossing point in the nuclei ^{40}Ca , ^{44}Ti , ^{62}Zn , and ^{74}Kr .

The nucleus-nucleus interaction potential (2) and condition (1) are applied to the prediction of the termination spins J_{term} of negative-parity bands built on the ground state in the nuclei ^{20}Ne , ^{24}Mg , ^{28}Si , ^{32}S , ^{36}Ar , $^{40,42}\text{Ca}$, ^{44}Ti , ^{54}Cr , ^{62}Zn , ^{74}Kr , and ^{102}Pd (Fig. 7). As examples, we obtain $J_{\text{term}}=19, 21, 29, 39,$ and 51 for the nuclei $^{40}\text{Ca} \rightarrow ^{36}\text{Ar} + ^4\text{He}$, $^{44}\text{Ti} \rightarrow ^{40}\text{Ca} + ^4\text{He}$, $^{62}\text{Zn} \rightarrow ^{58}\text{Ni} + ^4\text{He}$, $^{74}\text{Kr} \rightarrow ^{70}\text{Se} + ^4\text{He}$, and $^{102}\text{Pd} \rightarrow ^{98}\text{Ru} + ^4\text{He}$, respectively (see Figs. 3–7). Note that in the nuclei ^{44}Ti , ^{62}Zn , ^{74}Kr , and ^{102}Pd , the presently measured highest spin values within negative-parity band built on the ground state are $J^\pi = 13^-, 13^-, 35^-,$ and 21^- , respectively [26,27]. They are always smaller than our predicted J_{term} . In the case of ^{74}Kr the calculated J_{term} is close to the highest spin measured in the low-lying negative-parity band. In the cluster model [7–9] the termination spin for the ^{44}Ti nucleus is predicted at $J = 13$. However, the states with higher spin seem to be possible.

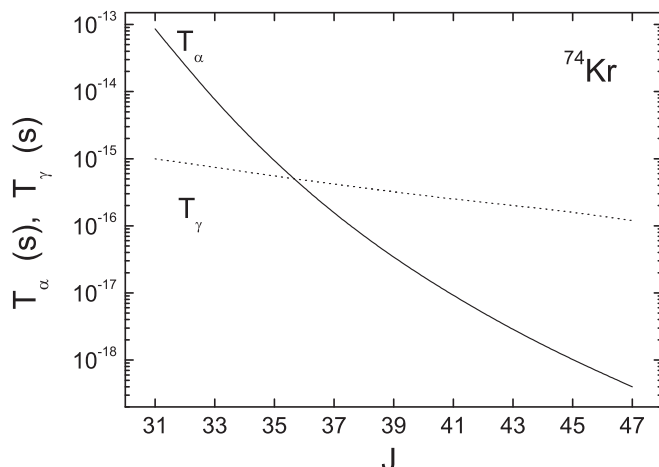


FIG. 6. Times of $E2$ transition and α decay as functions of angular momentum J for the indicated nucleus.

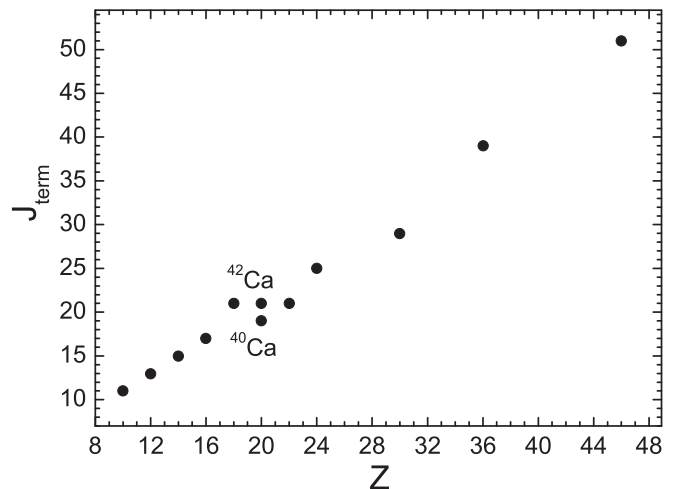


FIG. 7. The termination spin as a function of atomic number.

In Fig. 7, the J_{term} is almost linear dependent on the atomic number Z of nucleus, increasing by the factor of ~ 4.6 from $Z = 10$ to $Z = 46$. The differences between J_{term} in these α -cluster configurations arise because of the differences of their $B_R^{qf}(J=0)$ and moments of inertia (through the differences of R_m and R_b). The deformation of the heavy nucleus also comes into play through the R_m and R_b . For instance, for nuclei ^{42}Ca and ^{44}Ti , the barriers and moments of inertia [$\beta_1(^{38}\text{Ar}) = \beta_1(^{40}\text{Ca}) = 0$] of their α -cluster configurations are similar that results in the same termination spins, $J_{\text{term}} = 21$. The gain in $B_R^{qf}(J=0)$ for ^{36}Ar with respect to ^{42}Ca or ^{44}Ti compensates the loss in the moment of inertia leading to the same J_{term} .

After the γ emission ($E1$ or $E2$) from the negative-parity state with $J = J_{\text{term}} - 2$ [the positive-parity state with $J = J_{\text{term}} - 1$ or $J = J_{\text{term}} - 3$] to the negative-parity state with $J = J_{\text{term}} - 4$ [$J_{\text{term}} - 2$ or $J = J_{\text{term}} - 4$], the

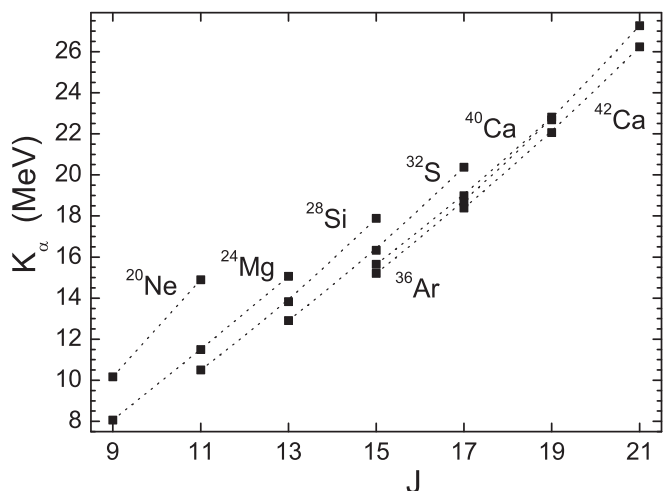


FIG. 8. The estimated average kinetic energies K_α of the alpha clusters released by the indicated nuclei at $J = J_{\text{term}}, J_{\text{term}} - 2,$ $J_{\text{term}} - 4$. The symbols related to the same nucleus are connected by dotted line.

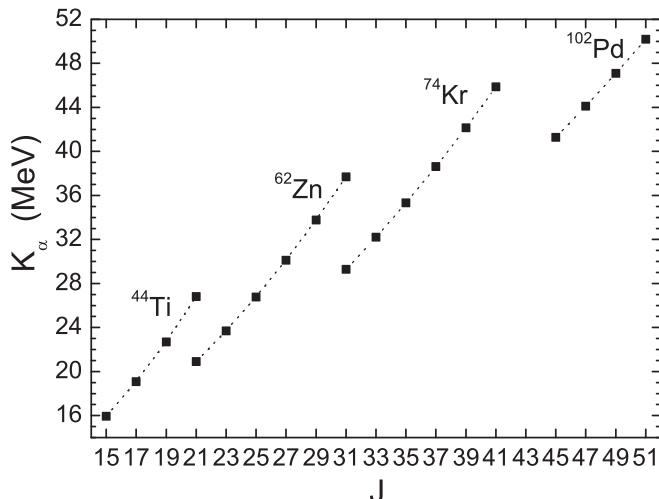


FIG. 9. The estimated average kinetic energies K_α of the alpha clusters released by the indicated nuclei at $J = J_{\text{term}}, J_{\text{term}} - 2, J_{\text{term}} - 4, \dots$. The symbols related to the same nucleus are connected by dotted line.

${}^A Z \rightarrow {}^{A-4} (Z-2) + {}^4\text{He}$ cluster configuration can decay into two fragments because the decay probability is somewhat high at J in the vicinity of J_{term} . By measuring the γ emission in coincidence with decay fragments of the alpha-cluster system, one can obtain a direct proof of the cluster feature of the negative-parity states. We think this correlation can be studied with a large gamma-ray detector array and an additional detector setup to register the fragments. One can also measure the average kinetic energy of the decay fragments. The estimated average kinetic energies,

$$K_\alpha = \frac{A-4}{A} \left[V(R_b, J=0) + \frac{\hbar^2 J(J+1)}{2\mathfrak{I}(R_b, \beta_i)} \right], \quad (7)$$

of alpha particle after the decay of cluster configuration at $J = J_{\text{term}}, J_{\text{term}} - 2, J_{\text{term}} - 4, \dots$ are presented in Figs. 8 and 9. Note that in the equations used the values of R_m and R_b depend on J . In Fig. 10, the $E2$ -transition energies between the negative-parity states with $J = J_{\text{term}} - 2, J_{\text{term}} - 4,$ and $J = J_{\text{term}} - 4, J_{\text{term}} - 6$ are shown as well.

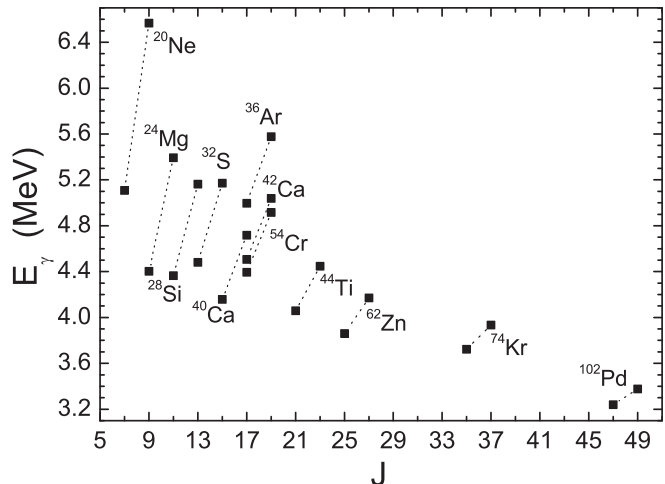


FIG. 10. The $E2$ -transition energy as a function of spin of indicated nuclei. The symbols related to the same nucleus are connected by dotted line.

IV. SUMMARY

Applying the cluster interpretation to the description of the negative-parity rotational band built on the nuclear ground state, the terminating spins $J = J_{\text{term}}$ for the nuclei ${}^{20}\text{Ne}$, ${}^{24}\text{Mg}$, ${}^{28}\text{Si}$, ${}^{32}\text{S}$, ${}^{36}\text{Ar}$, ${}^{40,42}\text{Ca}$, ${}^{44}\text{Ti}$, ${}^{54}\text{Cr}$, ${}^{62}\text{Zn}$, ${}^{74}\text{Kr}$, and ${}^{102}\text{Pd}$ were determined. We predicted that the physical origin of the termination of negative-parity rotational band is the decay of the alpha-cluster configuration into two fragments. To verify in the experiments the cluster origin of the low-lying negative parity states, one could suggest a measurement of the γ emission from the negative-parity state with $J = J_{\text{term}} - 2$ [positive-parity state with $J = J_{\text{term}} - 1$ or $J = J_{\text{term}} - 3$] to the negative-parity state with $J = J_{\text{term}} - 4$ [$J = J_{\text{term}} - 2$ or $J = J_{\text{term}} - 4$] in coincidence with decay fragments of the corresponding alpha-cluster configuration. The average total kinetic energies of decay fragments at $J \leq J_{\text{term}}$ and the $E2$ -transition energies between the negative-parity states with J near J_{term} were estimated.

ACKNOWLEDGMENTS

G.G.A. and N.V.A. acknowledge partial financial support from the HIC for FAIR guest funds of the Justus-Liebig University Giessen, Heisenberg-Landau programme (Dubna), and Alexander von Humboldt-Stiftung (Bonn). This work was partly supported by RFBR.

- [1] L. P. Gaffney *et al.*, *Nature (London)* **497**, 199 (2013).
 [2] B. Buck, C. B. Dover, and J. P. Vary, *Phys. Rev. C* **11**, 1803 (1975).
 [3] K. F. Pal and R. G. Lovas, *Phys. Lett. B* **96**, 19 (1980).
 [4] F. Iachello and A. D. Jackson, *Phys. Lett. B* **108**, 151 (1982); M. Gai, J. F. Ennis, M. Ruscev, E. C. Schloemer, B. Shivakumar, S. M. Sterbenz, N. Tsoupas, and D. A. Bromley, *Phys. Rev.*

- Lett.* **51**, 646 (1983); H. Daley and F. Iachello, *Phys. Lett. B* **131**, 281 (1983); H. Daley and J. Barret, *Nucl. Phys. A* **449**, 256 (1986).
 [5] F. Michel, G. Reidemeister, and S. Ohkubo, *Phys. Rev. Lett.* **57**, 1215 (1986).
 [6] O. F. Nemetz, V. G. Neudachin, A. T. Rudchik, Yu. F. Smirnov, and Yu. M. Tchuvil'sky, *Nucleon Clusters in Atomic Nuclei*

- and Multi-Nucleon Transfer Reactions* (Naukova Dumka, Kiev, 1988).
- [7] A. C. Merchant, K. F. Pal, and P. E. Hodgson, *J. Phys. G: Nucl. Part. Phys.* **15**, 601 (1989).
- [8] B. Buck, A. C. Merchant, and S. M. Perez, *Phys. Rev. Lett.* **76**, 380 (1996); *Phys. Rev. C* **57**, R2095 (1998); **58**, 2049 (1998); **59**, 750 (1999); **61**, 024314 (2000).
- [9] B. Buck, A. C. Merchant, M. J. Horner, and S. M. Perez, *Nucl. Phys. A* **673**, 157 (2000); B. Buck, A. C. Merchant, S. M. Perez, and H. E. Seals, *J. Phys. G: Nucl. Part. Phys.* **31**, 1499 (2005).
- [10] J. Cseh, A. Algora, J. Darai, and P. O. Hess, *Phys. Rev. C* **70**, 034311 (2004); J. Darai, J. Cseh, and D. G. Jenkins, *ibid.* **86**, 064309 (2012).
- [11] M. Spieker, S. Pascu, A. Zilges, and F. Iachello, *Phys. Rev. Lett.* **114**, 192504 (2015).
- [12] A. Volya and Yu. M. Tchuvilsky, *Phys. Rev. C* **91**, 044319 (2015).
- [13] B. Buck, A. C. Merchant, and S. M. Perez, *At. Data Nucl. Data Tables* **54**, 53 (1993).
- [14] T. M. Shneidman, G. G. Adamian, N. V. Antonenko, R. V. Jolos, and W. Scheid, *Phys. Lett. B* **526**, 322 (2002); *Phys. Rev. C* **67**, 014313 (2003).
- [15] G. G. Adamian, N. V. Antonenko, R. V. Jolos, and T. M. Shneidman, *Phys. Rev. C* **70**, 064318 (2004); T. M. Shneidman, G. G. Adamian, N. V. Antonenko, and R. V. Jolos, *ibid.* **74**, 034316 (2006).
- [16] T. M. Shneidman, G. G. Adamian, N. V. Antonenko, R. V. Jolos, and S.-G. Zhou, *Phys. Rev. C* **92**, 034302 (2015).
- [17] G. G. Adamian, N. V. Antonenko, R. V. Jolos, Yu. V. Palchikov and W. Scheid, *Phys. Rev. C* **67**, 054303 (2003); G. G. Adamian, N. V. Antonenko, R. V. Jolos, Yu. V. Palchikov, W. Scheid, and T. M. Shneidman, *ibid.* **69**, 054310 (2004).
- [18] S. N. Kuklin, T. M. Shneidman, G. G. Adamian, and N. V. Antonenko, *Eur. Phys. J. A* **48**, 112 (2012).
- [19] G. G. Adamian, N. V. Antonenko, and W. Scheid, in *Clusters in Nuclei*, edited by Christian Beck, Lecture Notes in Physics 848 (Springer-Verlag, Berlin, 2012), Vol. 2, p. 165.
- [20] A. S. Zubov, V. V. Sargsyan, G. G. Adamian, and N. V. Antonenko, *Phys. Rev. C* **88**, 034607 (2013).
- [21] G. G. Adamian, N. V. Antonenko, R. V. Jolos, S. P. Ivanova, and O. I. Melnikova, *Int. J. Mod. Phys. E* **05**, 191 (1996).
- [22] A. B. Migdal, *Theory of Finite Fermi Systems and Applications to Atomic Nuclei* (Wiley, New York, 1967).
- [23] S. Raman, C. W. Nestor Jr., and P. Tikkanen, *At. Data Nucl. Data Tables* **78**, 1 (2001).
- [24] S. Åberg and L.-O. Jönsson, *Annu. Rev. Nucl. Part. Sci.* **40**, 439 (1990); S. Åberg, *Nucl. Phys. A* **557**, 17 (1993); *Z. Phys. A* **349**, 205 (1994); J. Dudek, *Prog. Part. Nucl. Phys.* **28**, 131 (1992).
- [25] T. M. Shneidman, G. G. Adamian, N. V. Antonenko, S. P. Ivanova, and W. Scheid, *Nucl. Phys. A* **671**, 119 (2000).
- [26] <http://www.nndc.bnl.gov/>.
- [27] J. J. Valiente-Dobón *et al.*, *Phys. Rev. Lett.* **95**, 232501 (2005).